IEEE Access
Multidisciplinary ⋮ Rapid Review ⋮ Open Access Journal

Received 18 July 2022, accepted 17 August 2022, date of publication 26 August 2022, date of current version 2 September 2022.

Digital Object Identifier 10.1109/ACCESS.2022.3201824

RESEARCH ARTICLE

Elastic Tactile Sensor Skin on Double-Curved Surfaces for Robots and Wearables

PHILIPP RUPPEL, NORMAN HENDRICH, AND JIANWEI ZHANG
Department of Informatics, Universität Hamburg, 22527 Hamburg, Germany

Corresponding author: Philipp Ruppel (ruppel@informatik.uni-hamburg.de)

This work was supported in part by the German Research Foundation (DFG) through the Project Crossmodal Learning under Grant SFB TRR 169.

ABSTRACT Tactile perception is an important modality for dexterous manipulation, but faces unique challenges in that the sensor has to wrap around the system. Biological skin solves these problems extremely well. Not only can it detect contacts, but it also grows on complex three-dimensional shapes, stretches with underlying soft tissue and around joints, and leaves enough space inside for other organs. Previous artificial sensors could only achieve different subsets of these features. We present a novel tactile sensor skin which is completely made from elastic silicone rubber and can stretch to multiple times its original length without damage. It can be produced in three-dimensional double-curved shapes, is thin enough to accommodate other robot components or human body parts, and it can measure forces and locations of multiple simultaneous contacts. We develop production methods and material formulations, algorithms for computer-aided design, compact readout electronics using small, low-power FPGAs, firmware, and software.

INDEX TERMS Tactile sensors, robot sensing systems, robot learning, soft robotics.

I. INTRODUCTION

Humans and robots manipulate objects through physical contacts. Robots usually do so indirectly, based on object and joint positions, and in some cases joint torques. Since interacting with the real world always involves a degree of uncertainty, it would be desirable to measure contacts directly. Not only should the sensor be able to measure force distributions, but more importantly, in order to do so, the sensor must be able to cover all surfaces where relevant contacts might happen. Biological skin appears extremely well adapted to these problems [1]. It can grow on complex three-dimensional shapes to measure contact information, stretch with underlying soft tissue and around joints, and it leaves most of the internal volume for other organs.

Previous artificial tactile sensors could only offer different subsets of these features [2], [3] (see table 1). Matrix sensors can be thin and bendable, but are typically flat and not stretchable. Fabric-based sensors have relatively low spatial resolutions, can only stretch by at most a few percent, and are also usually produced as flat sheets. Camera- and liquid-based sensors can have curved and elastic surfaces, but the internal volume is occupied by optics or electronics and cannot be used in other ways.

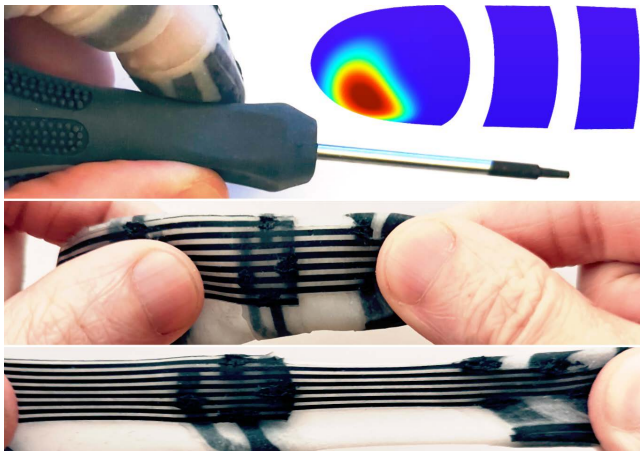

FIGURE 1. We present a novel artificial sensor skin that can wrap around three-dimensional shapes and is highly elastic (middle, bottom). It can be used on robots or wearables (top-left) to measure contact information (top-right).

The associate editor coordinating the review of this manuscript and approving it for publication was Xiaokang Yin.

We present a novel artificial tactile sensor skin which is highly stretchable, can be produced in complex three-dimensional shapes, only covers the surface, and can measure force distributions with multiple simultaneous contacts (see figure 1). Our sensor skin could be applied to robots directly to improve sensing and control. It could also be used on gloves or other wearables to record data for imitation learning and to study human grasping and manipulation strategies.

We present methods and tools for designing and manufacturing matrix sensors on three-dimensional double-curved surfaces. To build devices that are fully stretchable, we develop suitable electrically conductive silicone materials. Our PCB and VLSI designs allow for efficient readout with minimal external components. In a distributed architecture, miniaturized boards are placed close to the sensors. To read sensors across deformable parts in centralized architectures, we develop stretchable silicone cables and a board design with additional amplifiers and more channels (up to 256 cells per board). We build two prototypes and perform first manipulation experiments. A multimodal fingertip integrates a double-curved elastic skin and a small local readout board on the fingernail, which carries an additional IMU and an LED for motion tracking. Our elastic finger sensor also measures contacts on the middle and proximal phalanges and is completely made from stretchable materials, without any rigid parts. It is read via an elastic silicone cable. The readout board can be placed on the wrist. We perform several experiments to characterize the sensor response.

In the following, we first summarize related work. We then introduce our design and production methods, and our material formulations. We describe PCB and VLSI designs, followed by prototypes and experiments. We close with conclusions and ideas for future research.

II. RELATED WORK

A. LIQUID- AND CAMERA-BASED TACTILE SENSORS

Fishel *et al.* [4] developed a tactile fingertip with an elastic double-curved silicone skin. The BioTac sensor is a popular choice among roboticists, but it is not suitable for covering entire robots, soft robots or human body parts in tactile skin, since the internal volume is occupied by conductive liquid and a rigid core with sensing elements. The relatively large thickness leads to a non-trivial relationship between contacts and measurements. For accurate interpretation, these effects have to be modeled using artificial neural networks or finite element analysis [18], [19].

Camera-based tactile sensors have recently been receiving a great deal of attention [11], [14], [15], [20], [21], [22]. A soft elastomer skin is placed in front of a camera module. Since the internal volume has to be mostly empty and large enough to accommodate electronics and lenses, these devices are restricted to similar applications as the BioTac sensor.

B. TACTILE MATRIX SENSORS

Thin tactile matrix sensors can be constructed from metal foils as electrodes and polymer dielectrics [13], piezo-resistive polymers [17], or liquid droplets [6] in-between. These devices can be flexible and relatively accurate, measurements are comparably easy to interpret, but the sensors are typically flat and the electrode material is not stretchable. Flexible tactile sensors can be bent to produce cylindrical sensors [23], but double-curved surfaces cannot be instrumented by simply bending a flat sensor matrix.

C. WEARABLE TACTILE SENSORS

Tactile sensors have been mounted on instrumented gloves [8], [16], [24]. Depending on the technology, these designs still suffer from limited elasticity, low resolution, and limited surface coverage. Sundaram et al. attach a higher-resolution but flat sensor matrix to a glove [7]. The sensor is bendable, but only covers the inside of the hand. Battaglia et al. use 3D-printed shells and a force-torque sensor to detect contacts [10]. The device can be used to estimate the force and location of one contact, but it is not stretchable, only covers the tip, and is relatively large and heavy.

D. MODULAR SENSOR SKIN

Robots can be covered with networks of individual tactile sensor modules [12]. Current designs are still rigid and relatively large (multiple centimeters). For a general-purpose elastic sensor skin, the components would have to be orders of magnitude smaller, and would have to be embedded in an elastic skin with stretchable electrical connections.

E. STRETCHABLE ELECTRONICS

With carbon black as a conductive filler, it is possible to produce electrically conductive silicone rubber. This has been used in previous work to construct elastic strain sensors [25]. Conductive hydrogels can also be used, but degrade over time [26], [27]. Other researchers experiment with conductive liquids in microfluidic channels or dispersing conductive liquids in elastomers [28]. However, conductive liquids, especially metals that are liquid around room temperature, lead to safety and reliability issues. Mercury can be toxic, lithium-sodium alloy is highly flammable and reacts violently with water [29], and gallium (or its alloys) corrode other metals such as aluminum. The possibility of accidental release due to damage should always be considered. Having to electrically contact conductive liquids without leakage poses additional problems. Electrolytic solutions have lower conductivity, requiring comparably thick channels, which would have to be stabilized against compression. Otherwise, one contact at one location in a tactile sensor would interrupt the circuit connecting a sensing element in a different location. Electrolytes are also corrosive and can decompose under electrical current. New types of synthetic nano particles, such as graphene and carbon nanotubes, have recently become a popular topic in the academic literature. However, these materials are not only expensive, but their effects on human health and on the environment are still a matter of debate [30], [31]. Wang *et al.* use carbon nanotubes to create electrical connections that can be stretched by up to 400 % [32]. Danial *et al.* report a

TABLE 1. Our tactile sensor skin can be built in three-dimensional double-curved shapes, only covers the surface to leave space inside for other components, and is not only bendable but also highly stretchable. To the best of our knowledge, related works only provide different subsets of these features.

	Double-curved	Bendable	High elasticity	Surface only	Principle
Ours	Yes	Yes	Yes	Yes	Capacitive
BioTac [4]	Yes	No	Yes	No	Resistive
Tekscan [5]	No	Yes	No	Yes	Piezo-resistive
Pan et al. [6]	No	Yes	No	Yes	Electrolytic
Sundaran et al. [7]	No	Yes	No	Yes	Piezo-resistive
Bielefeld Glove [8]	No	Yes	No	No	Piezo-resistive
Bielefeld Fingertip [9]	Yes	No	No	No	Piezo-resistive
Thimble Sense [10]	Yes	No	No	No	Resistive
GelSight [11]	No	No	Yes	No	Optical
Hex-o-skin [12]	No	No	No	No	Optical
Lee et al. [13]	No	Yes	No	Yes	Capacitive
Facebook Digit [14]	No	No	Yes	No	Optical
Insight [15]	Yes	No	Yes	No	Optical
Teaching glove [16]	No	Yes	No	Yes	Piezo-resistive
Low-cost matrix [17]	No	Yes	No	Yes	Piezo-resistive

maximum elongation of 98 % and resistances in the kiloohm range for a conductive silicone with a reduced graphene oxide filler [33]. Bountry *et al.* [34] attach a pressure sensor to a stretchable strain sensor. However, the pressure sensor itself is not significantly stretchable.

F. SILICONE ELASTOMERS

Elastic materials can be created from siloxanes, chains of alternating silicon and oxygen atoms with organic groups on the sides and ends. Some of these groups may have special functions and can be reacted to increase the length (chain extenders) and connect the chains into networks (crosslinkers). Pure silicones have relatively bad mechanical properties and easily break under pressure or tension. The performance can be enhanced by adding fillers, often nano-particles. Fumed silica is used to improve mechanical strength. Carbon black is electrically conductive. The final material properties can be tuned via the types and ratios of siloxanes and fillers. Existing commercial products often contain further additives, such as plasticizers and internal release agents, and are not always suitable for robotics applications [35]. New high-elongation silicones have recently been developed. Some authors report maximum elongations at break of up to 5000% under ideal conditions [36], [37]. It has been estimated that artificial skin may have to stretch by 500% if attached to a human finger joint and that modern silicones should theoretically be the best material choice for this application [36].

G. OWN PREVIOUS WORK

In our previous work, we built gloves with simple fabric-based piezo-resistive tactile sensors with one channel per fingertip [16]. Tactile data from the gloves was then used for teaching dexterous manipulation tasks to robots by demonstration. Human teachers showed the desired behavior with their own hands and real objects, while the system recorded motions and tactile information. The data was used to train artificial neural networks and the learned policies were executed successfully on real robots. However, the glove could not track rolling contacts, and the sensor material was found too rigid and too slippery, resulting in sub-optimal human motions.

We also developed methods for efficient learning in simulation. We trained the policy networks to generate contact points and contact forces while minimizing a physical consistency loss. This helped to overcome local minima and allowed us to learn neural network policies for dexterous manipulation tasks directly through gradient-based optimization [38]. We expect that the learned contact information could be used together with tactile sensor skin to improve sim-to-real transfer.

III. DOUBLE-CURVED SENSOR MATRICES

A. WORKING PRINCIPLE

Our tactile sensor skin is completely made from elastic silicone rubber, some of which is electrically conductive. Two sets of conductive silicone traces are arranged to intersect each other, forming a matrix of force-sensing variable capacitors. The traces are embedded in dielectric silicone, with small compressible cavities between the layers. If varying excitation voltages are applied to one set of traces, electrical currents are coupled into the other set of traces and can be measured. Under mechanical pressure, the capacitance of the affected taxel increases and a higher electrical current is coupled into the reception line. While traditional tactile matrix sensors are produced on flat surfaces, biological skin can grow around complex three-dimensional shapes, such as hands and fingers. We create sensor matrices directly in three-dimensional double-curved shapes using 3D-printed molds and jigs.

B. DESIGN PROCESS

We first design a virtual model of the sensor. The shape is specified as a subdivision surface and the electrode layout is defined by modeling two perpendicular sets of traces. For the prototypes shown in this paper, we model the shapes in Blender.[1] The traces are then subdivided and projected onto

[1] Blender, https://www.blender.org/

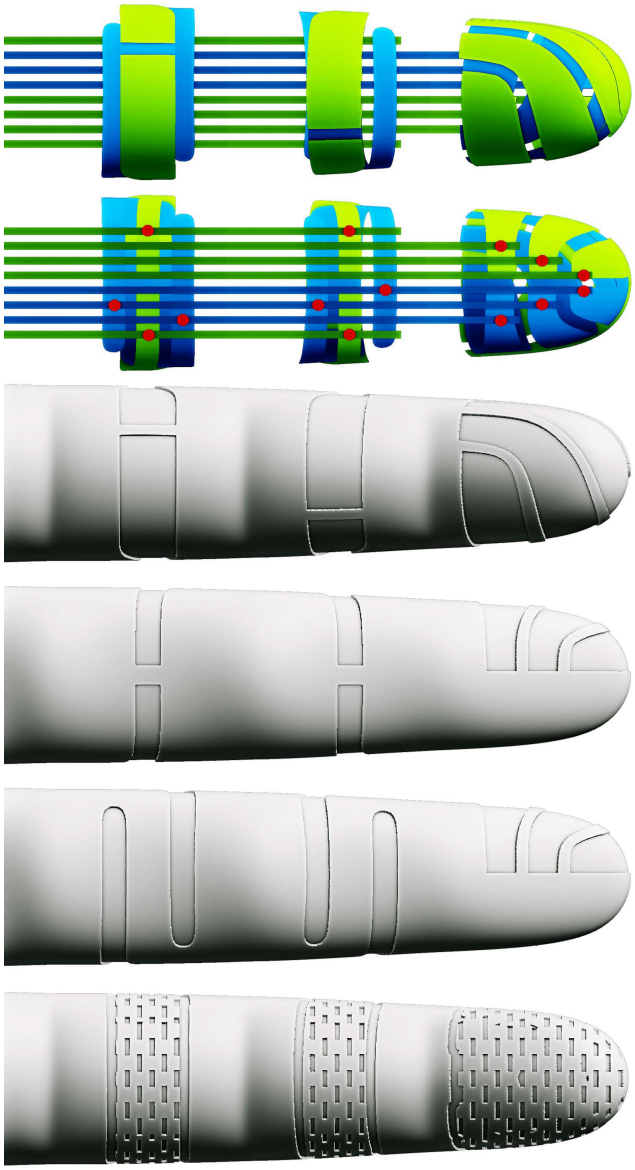

FIGURE 2. CAD models for a tactile finger sensor. Electrical layout (top) with transmission (green) and reception lines (blue), and vertical vias (red). Assembly jigs (middle), dielectric mold (bottom).

the skin. For each vertex of a subdivided trace, the closest point on the skin is found and the vertex is moved to the new position. The traces can thus be specified by simply modeling a rough low-resolution cage around the skin. The parts, molds and jigs for manufacturing the sensor are generated from this information procedurally (figure 2 and 3, section III-D-III-F).

C. SUBSTRATE

The sensor cells are produced on a non-conductive silicone substrate. We print a model of the object that we want to cover in tactile sensor skin on a regular FFF printer in PLA. To smooth the surface, to close holes and to improve heat resistance, we dissolve a small amount of cellulose acetate in acetone and apply the mixture to the surface. We then

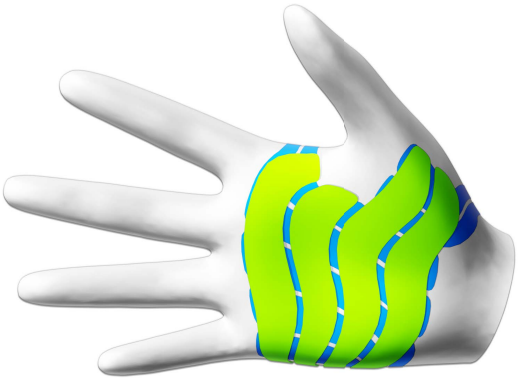

FIGURE 3. CAD model of a palm sensor for a tactile sensor glove. Conductive traces (blue and green) wrap around a three-dimensional hand model (grey) to form a matrix sensor with an irregular shape and a double-curved surface.

mix a liquid silicone rubber (section IV-D), pour it over the mold and let it cure. The curing process can be accelerated by increasing the temperature. For the prototypes shown in this paper, we heat to 100°C for one hour. After curing, we apply a small amount of powdered calcium carbonate to the silicone as a separating agent and remove the skin.

D. CONDUCTIVE TRACES

After projecting the traces onto the base model, we unwrap each trace onto a plane and pack the shapes into a small area for manufacturing. See figure 4 for an example (tactile finger sensor). We develop algorithms to solve these problems and implement a command line tool, which loads a 3D mesh file and generates an SVG file with the parts.

Unwrapping three-dimensional shapes is a common operation in 3D modeling. Current algorithms typically try to preserve angles (conformal maps). We want to minimize stretch for our application, avoiding unnecessary mechanical stresses, which might otherwise complicate assembly and make the skin stiffer. Standard 3D modeling packages like Blender[1] support angle-preserving methods but not fully automated stretch-minimizing unwrapping. We solve the problem using a sequential least-squares approach with randomization to overcome local minima (see figures 4 and 5). After unwrapping, we pack all parts into a small area to minimize waste during manufacture (see appendix XI).

To manufacture the conductive traces and pads, we first cast a conductive silicone film (section IV-B) onto a PET sheet. We then cut the parts using a cutting plotter[2] according to the generated SVG file. The conductive film adheres well enough to the PET sheet to be cut, but the parts can still be removed without damage.

E. ASSEMBLY JIGS

The conductive parts are placed onto the skin using computer-generated 3D-printed assembly jigs (see figure 2). We start with the subdivision surface model and extrude all parts that

[2]Silhouette Portrait 2, https://silhouetteamerica.com/, via inkscape-silhouette, https://github.com/fablabnbg/inkscape-silhouette

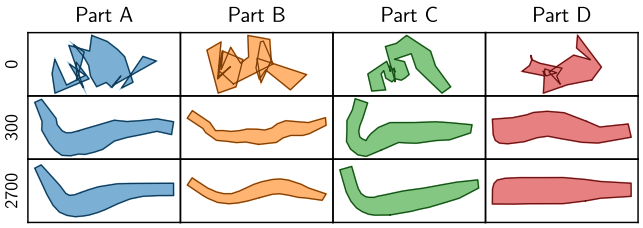

FIGURE 4. Our tool path generator unwraps the conductive parts for a double-curved fingertip sensor while minimizing stretch. Each column corresponds to one conductive part and each row to one iteration.

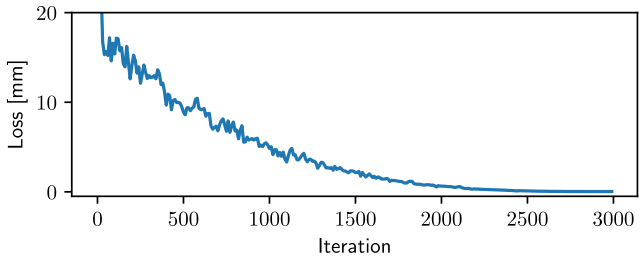

FIGURE 5. We unwrap the conductive parts through an optimization-based process that minimizes stretch (Y axis) over multiple iterations (X axis).

lie under conductive traces inwards, along the negative of the normal. We generate two separate fixtures, one for placing the transmission lines and one for the reception lines. The models are printed in PLA on an FFF printer.

We glue the conductive traces into the corresponding slots on the fixtures using a custom silicone adhesive (section IV-C). After the adhesive is cured, we apply a thin layer of silicone (section IV-D) and pull the previously cast layer of skin over the jig. When the silicone is cured, the skin can be pulled off and the traces separate from the jig while adhering to the skin. The same fixtures can be re-used many times. The whole process is performed twice, once to create an outer layer with traces on the inside and again to create an inner layer with traces on the outside that are perpendicular to the traces on the outer layer.

Our technique makes it possible to create and accurately place thin layers of conductive silicone with uniform thickness on elastic silicone skins using off-the-shelf FFF printers and cutting plotters.

F. DIELECTRIC LAYER

Both electrode layers are separated by a compressible dielectric structure to form force-sensing variable capacitors. While our silicone materials are elastic and stretchable, compressing silicone rubber into a smaller volume would require extremely high forces. We therefore create structures with air-filled cavities. We experiment with different designs and production methods. Closed air-filled cells provide excellent repeatability, as the behavior mainly depends on the compression of a gas, but they have lower sensitivity and respond to stretching. Open cells or silicone columns with a network of air pockets can be more sensitive and show less crosstalk when stretched.

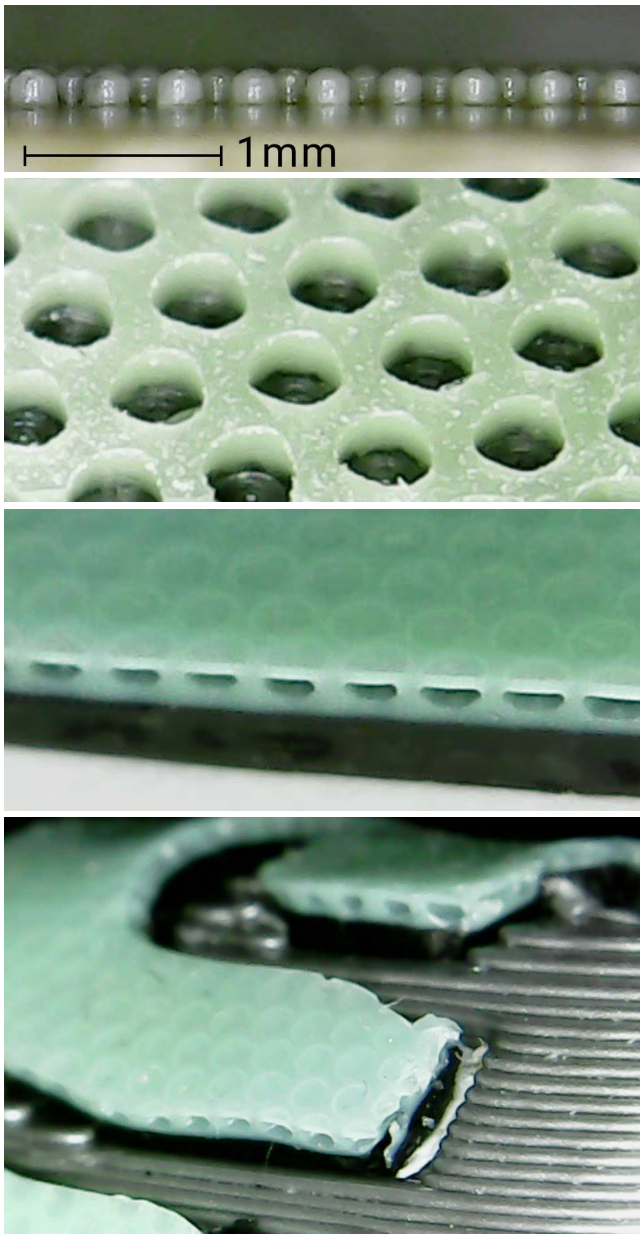

FIGURE 6. We cast a mold (top) for structuring a closed-celled dielectric. Each bump has a height of approximately 0.2 mm. The mold is used to create a cell structure (second from top) and the cells are closed with a silicone film (third). The sheets are cut into parts using a cutting plotter and glued to a 3D-printed assembly jig (bottom). The steps on the jig are 3D printing layers.

A relatively simple approach is to produce silicone sponges using soluble fillers. We mix silicone with soluble particles (e.g. sodium chloride / table salt), cast the mixture into sheets, cure the silicone, stretch and press the sheets to break the cells open, and then dissolve the salt. However, we were not satisfied with the reproducibility. It is hard to control the exact density of the sponge structure, and it is even harder to control whether or not the cells should be open or closed. When creating open cells, another disadvantage is that the cells are round and therefore show a relatively large compression when stretched. While we do not use this approach anymore, it may

still be of interest as it is easy to replicate and well suited for first experiments.

To produce a more precise closed cell structure, we use a molding process. We drill a set of holes aligned in a ''honeycomb'' structure into an aluminum plate with a CNC mill. We then cover the plate with polyurethane resin, place it in a vacuum chamber to remove air bubbles, release the vacuum and let the resin cure. See figure 6 for a micrograph of the cast polyurethane mold. In our experience, first milling the positive and then creating a negative casting is faster and yields better results in this case than directly milling the negative mold. Before cutting the conductive silicone films into parts and gluing the parts to the assembly jig, we pour a layer of non-conductive silicone (section IV-D) over the dielectric mold, remove air bubbles in a vacuum chamber, and then press the PET carrier with the conductive silicone film onto the dielectric mold. After curing, we remove the structure from the mold and are left with a conductive silicone film with an open honeycomb structure on top. To close the cells, we apply a thin layer of silicone of about 50 μ m onto a flat plate, let it cure, coat the film in fresh silicone, place the PET carrier with the conductive film and honeycomb structure on top (with the cells facing down), and press both sides together between two flat metal plates. We obtain a conductive silicone film on a PET carrier with a closed-celled dielectric honeycomb structure (figure 6), which can be processed as described above. The honeycomb structure is only applied to either the inner or the outer layer and both layers are glued together.

To produce an open cell structure, we first create an outer and an inner layer with conductive traces as described above, without the closed cells. We then generate another 3D-printed mold, which defines the dielectric pattern (see figure 2), apply non-conductive silicone, and pull the outer skin over the mold. When the silicone is cured, we pull the inner skin over one of the smooth molds used in the beginning to cast the substrates, apply a thin coating of fresh silicone, and pull the outer layer over the inner one to glue both layers together. The open cell structure is produced directly in its final shape to avoid obstructing cavities with excess silicone during assembly. For many applications, the structure size should be well below 1 mm for the sensor to be thin enough. To still resolve the pattern on a regular FFF printer, we use a brick structure and align it with the 3D printing layers. The pattern is only generated under and around the sensor cells. For each vertex of the tessellated subdivision surface model, we check if the distances to the next transmission and reception lines are below a threshold and if it lies on one of the layer-aligned bricks. If both is the case, we move it by a small distance along the normal. The brick pattern is projected onto the surface through regular biplanar texturing.

G. ELASTIC FLAT CABLES

In some cases, we want to place the readout electronics in a different location away from the sensor, with elastic skin in-between. We create stretchable flat cables that are, like our sensor itself, completely made from elastic silicone. We first cast a conductive film, as described in section IV-B, onto a PET sheet. The silicone is cut into parallel wires using a cutting plotter[2]. Conductive material left between the wires is removed. We then pour dielectric silicone over the sheet with the silicone wires and spread it using a doctor blade, filling the space between the traces.

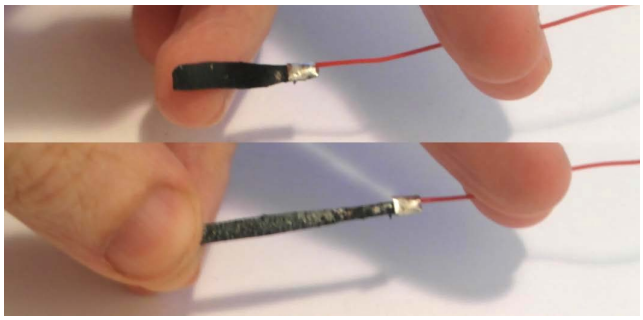

FIGURE 7. A metal pad is glued to a conductive silicone part and a wire is soldered to the pad. The silicone can be stretched without damaging the joint.

One end of the cable is connected to the readout board using a mechanical clamp. This requires the distance of the traces to be constant and to not change under pressure. To maintain a constant pitch, we attach a small inelastic stiffener to one end. We use a PET film with a thickness of 0.3 mm, roughen the surface with fine sandpaper, apply a primer (Wacker G790[3]), cut it to the correct shape, and glue it with non-conductive silicone to one end of the cable. The stiffener only has to cover a small part of the cable (1cm or less).

Finally, we remove the cable from the PET sheet and temporarily wrap the stiffened end in adhesive tape to protect the conductive pads from being covered in non-conductive silicone. We then apply silicone adhesive (section IV-C) to the lower side of the cable and glue it to the skin.

H. VERTICAL VIAS

The other end of the elastic silicone cable has to connect to the conductive traces in the sensor (see figure 2). We join the corresponding traces on both layers through vertical via. For every connection, we punch a hole with an injection needle. We then fill the holes with conductive silicone (section IV-B) and let it cure. Finally, we apply a thin coating of non-conductive silicone to each via for electrical insulation.

I. SOLDER PADS

In some cases, we want to integrate the readout electronics close to the sensor. We glue small metal pads onto the conductive silicone traces and solder the pads onto the circuit boards. We start with a thin copper sheet (100 μm), clean it with fine sand paper and then acetone, electrolytically coat

[3]Wacker Primer G790, https://www.wacker.com/h/silicone-rubber/primer-for-silicone-rubber/wacker-primer-g-790/p/000023017

TABLE 2. We develop special electrically conductive (A-D) and adhesive (B, E) silicone formulations for producing stretchable tactile sensor skin. Each of the columns A to E lists the composition of one mixture. The name and other information are listed in the corresponding rows under "Precursors". For each formulation, all parts except for the catalyst can be mixed once and then stored for later use. The silicone begins to cure once the catalyst is added.

Composition [% by weight]					Precursors			
A	B	C	D	E	Name	Function	CAS	Stoichiometry
–	–	57.9	31.0	81.6	Vinyl-terminated PDMS 2000 cSt [6]	Base	68083-19-2	0.1 mmol/g vinyl
74.3	68.2	–	–	–	Vinyl-terminated PDMS 20000 cSt [6]	Base	68083-19-2	0.04 mmol/g vinyl
–	–	1.700	0.912	2.40	Hydride-terminated PDMS 5 cSt [6]	Chain extender	70900-21-9	2.6 mmol/g hydride
0.87	9.1	0.427	0.228	0.60	Methylhydrosiloxane-DMS copolymer [6]	Crosslinker	69013-23-6	3.2 mmol/g hydride
24.8	22.7	–	–	–	Carbon black / PP802 [5]	Filler	1333-86-4	–
–	–	39.9	19.4	–	Carbon black [4]	Filler	1333-86-4	–
0.002	0.002	0.01	0.01	0.002	Karstedt catalyst solution [6]	Catalyst	68478-92-2	–
–	–	–	48.5	–	Hydrocarbons $C_{10} - C_{13}$	Solvent	649-327-00-6	–
–	–	–	–	0.01	Tetravinyltetramethylcyclotetrasiloxane [6]	Delayer	2554-065	–
–	–	–	–	17.7	Hydrophobic fumed silica [7]	Filler	68611-44-9	–
Conductive				Dielectric				

one side with tin and apply a primer (G790[3]) to the other side. We then cover the tin-coated side with regular adhesive tape for protection and apply a thin layer of electrically conductive silicone (section IV-B) to the primed side. The sheet is cut into small pads, which are then glued with conductive silicone onto the conductive traces in the sensor. When the silicone is cured and the protective tape is removed, the pads are soldered to the readout board. Our silicone formulations are heat-resistant enough to withstand lead-free solder temperatures. The silicone parts can be stretched without damaging the joints (see figure 7).

J. POST CURING

When the sensor skin has been fully assembled, we cover it with aluminum foil to prevent local overheating and bake it for a few hours at 140°C to ensure that the silicone is fully cured and to remove any potentially remaining volatiles. Finally, a small amount of powder can be applied to adjust the amount of friction (talcum, baby powder, etc.).

IV. MATERIALS

A. CONDUCTIVE TPU

During our first experiments, we used a conductive TPU [39] for the conductive traces. While the sensors worked in principle, the material was too stiff and suffered from plastic deformation when stretched.

B. CONDUCTIVE SILICONE

To improve the material properties, we switched to silicone-based formulations. Initially, we simply mixed several commercially available two-part silicones with different types of carbon black. Even at elevated temperatures, the mixtures only cure very slowly or not at all, the conductivity is usually too low for our applications, and the added carbon black turns the resin into very thick pastes, which are hard to mix and process. Carbon black typically contains impurities, which can delay or inhibit the curing process, particularly for addition-cure silicone. Existing silicone formulations also already contain fillers (fumed silica, powdered minerals, etc.) and the viscosity rises strongly with filler content, so adding a large amount of carbon black to a formulation that already contains fillers can make the silicone practically unusable. After many trials, we find one combination with a commercially available molding silicone [40] that works well enough to build first silicone-based prototypes. The properties also depend heavily on the type of carbon black. While mixing commercial molding silicone with a standard lamp black[4] resulted in very bad conductivity, a different carbon black (pigment, source unknown) led to significantly better conductivity. We hypothesize that this may be due to particle size and/or impurities, so we obtain a special high-purity carbon black for food contact plastics (PP802 by PCBL Ltd.[5]) and the conductivity does indeed improve by orders of magnitude. We first individually mix three parts part A and three parts part B of TFC Type 2 silicone with 1 part each of PP802 carbon black (parts by weight), and shortly before use, mix both. The paste is pressed into a sheet between two pieces of PTFE foil and then cured for two hours at 120°C. The material has a maximum elongation of about 100% and a volume resistivity of 0.3 Ω m. The elasticity is already better than that of a standard non-conductive silicone that is often used for academic work [41] and the conductivity is almost an order of magnitude better than that of the conductive TPU used above.

We develop custom electrically conductive silicone formulations from scratch to improve the elasticity and conductivity further. Silicone elastomers with long chains are generally more stretchable, so we initially use a vinyl-terminated PDMS with a relatively high viscosity of 20.000cSt as the base. We add carbon black as a conductive filler (PP802[5], CAS 1333-86-4), a hydride-functional copolymer as a crosslinker (CAS 69013-23-6) and a catalyst (Karstedt's catalyst, CAS 68478-92-2). See table 2 (column A) for details. This formulation results in an elastic material that can be stretched without damage by 400%. Compared

[4]Carbon black, compressed, CAS 1333-86-4, https://www.pyropowders.de/sortiment/holzkohlepulver-kohlenstoff/

[5]Food Contact Royale Black PP802, CAS 1333-86-4, PCBL Limited, https://www.pcblltd.com/product/food-contact

to the conductive TPU used above, it is now not only more conductive but also softer and more stretchable.

The previous mixture was formulated with a stoichiometric ratio of vinyl to hydride groups close to one, resulting in a soft and elastic material. In some cases, we want to glue conductive silicone directly to metal parts to establish an electrical contact. For this purpose, we prepare a conductive glue with an excess of crosslinker and hydride groups (see table 2, column B). This formulation adheres well to certain metals including copper and aluminum. The strength of the bond can be increased further by about 50% using a primer (e.g. G790[3]). It should be noted that the higher stoichiometric ratio of the conductive glue also changes the elasticity, lowering the maximum elongation at break to approximately 100%. It should therefore only be used as an adhesive to glue conductive silicone parts to inelastic materials.

For casting elastic silicone parts, we can also start with shorter vinyl-functional siloxanes and grow these into longer chains using a hydride-terminated siloxane as a chain extender (see table 2, column C). This reduces the viscosity of the uncured silicone, it allows us to increase the carbon black content further, and we can use a regular cheap lamp black.[4]

For most conductive parts, we first cast a thin sheet and then cut the parts using a cutting plotter. The film is thin enough that we can lower the viscosity further by adding a solvent and later evaporating it, making the uncured mixture easier to process. We first mix isoalkanes (solvent) with a vinyl-terminated PDMS, a crosslinker, and a chain extender. We then disperse the carbon black. See table 2 (column D) for details. Since the viscosity is now relatively low, it can be mixed using a standard kitchen blender. The compound can be prepared once and then stored for later use. When a small amount of a platinum catalyst is added and the mixture is spread out as a film, the silicone begins to cure while the solvent evaporates. After about one hour, it should be placed in an oven and heated to 100°C for a few hours to remove any remaining solvent and to finish the curing process. These two steps should be performed in a well-ventilated area, ideally under a fume hood or outside. The resulting conductive silicone film has a volume resistivity of 0.025 Ωm and can be stretched by over 550 % without damage. It is an order of magnitude more conductive and about five times more stretchable than our first conductive silicone formulation, roughly two orders of magnitude more conductive and significantly more stretchable than the conductive TPU, more stretchable than related work using graphene [33] and carbon nanotubes [32], and even compared to many regular non-conductive silicones, it is equally or more stretchable [35], [41].

The siloxane chemicals were obtained from Nedform BV.[6] If some of the chemicals have to be substituted with different but similar ones, e.g. due to availability, it is particularly important to maintain the correct stoichiometric ratios (see table 2, stoichiometry). We mixed the high-viscosity formulations (table 2, columns A, B, C, E) for a few hours each with a Cloer ART-7001 and the low-viscosity formulation (table 2, column D) for about half an hour (plus repeated breaks for the motor to cool down) with a Switch On TB B0201.

C. DIELECTRIC ADHESIVE

We also create a non-conductive adhesive formulation to simplify the assembly process. The formulation is similar to standard molding silicones, but sticky enough to already hold parts in place in its uncured state. It consists of a vinyl-terminated polydimethysiloxane, a hydride-functional crosslinker, a hydride-terminated siloxane as a chain extender, hydrophobic fumed silica[7] as a reinforcing filler and to control the viscosity, and a small amount of a methyl-vinyl cyclosiloxane as a delayer. Shortly before use, a platinum catalyst is added. See table 2 (column E) for details.

D. BASE MATERIAL

Formulating silicone rubbers without special electrical properties is a well-studied problem, and many different products are already commercially available. To be compatible with our other addition-cure silicones, the base material should also be an addition-cure silicone (''platinum cure''). It is important to choose a type with low viscosity and high elasticity. Many formulations also contain release agents, which should be avoided to ensure good layer adherence. Non-reactive plasticizers should be avoided as well (check datasheets), as they would leak out over time and result in bad repeatability. We currently use ExSil 100[8] high-elongation silicone from Gelest. Some commercially available silicone formulations have a relatively long cure time at room temperature (e.g. about 1 day for ExSil 100). The curing process can be accelerated by raising the temperature, or by adding a small amount of additional catalyst (e.g. Karstedt's catalyst[9]).

V. READOUT

To measure the pressure distribution across the sensor matrix, we transmit an electrical signal along each row and measure the current that is coupled into each column. We use sine waves with one frequency for each transmission line as excitation signals. An FPGA generates PCM-coded wave functions and translates these into rate-coded binary signals through first-order delta-sigma conversion. The binary signals can optionally be amplified by external drivers. Since the conductive silicone traces show a significant resistance, the sensor itself acts as a low-pass filter and we use low-frequency excitation signals 1 kHz that are not significantly attenuated. Higher frequencies would show a higher voltage drop along the traces due to ambient capacitance, internal sensor capacitance, and mutual capacitance with objects close to the sensor. Delta-sigma converters typically

[6]Nedform BV, https://siliconesandmore.com

[7]Aerosil R 812 S, Evonik Industries AG, http://evonik.com
[8]ExSil 100, Gelest Inc., https://www.gelest.com/product/EM2-EX100/
[9]Karstedt's catalyst, CAS 68478-92-2, Thermo Fischer GmbH

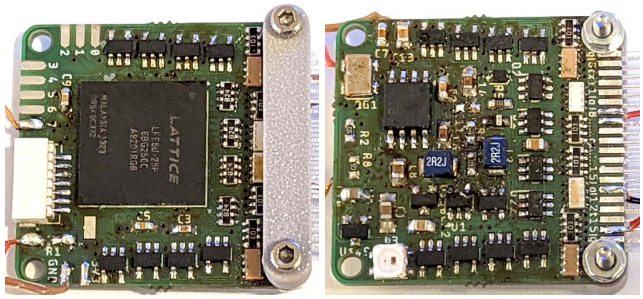

FIGURE 8. Our readout board with a size of 30 mm × 33 mm can simultaneously read 256 sensor cells.

require analog low-pass filters. In our case, these are not required since the sensor itself acts as an RC filter.

Electrical currents on the reception lines are measured through current-mode delta-sigma conversion. The FPGA attempts to keep each reception line at a fixed reference voltage while estimating the required current. The voltage on a reception line is compared to a reference voltage via an input pin. An output pin connects to the reception line through a resistor, allowing the FPGA to control the voltage level. Since the reception line is kept at a constant voltage, the output level is directly proportional to the current. Hysteresis on the input pin should be minimized, either by disabling hysteresis on a single-ended input (if supported), or by repurposing an LVDS input. We currently use 1 MΩ feedback resistors. For different sensor designs, the measuring range could be adjusted by changing the feedback resistors.

Letting the reception lines float and only measuring voltages would lead to severe crosstalk. The voltage change would depend on the ratios between the internal capacitance of the sensor cell, ambient capacitance, the capacitance of other sensor cells on the same reception line, and mutual capacitance with objects that are close to the sensor and exhibit a high dielectric permittivity (e.g. fingers). We avoid these issues by driving the transmission lines in voltage mode and holding the reception lines at a constant voltage while measuring the current. The transmission lines could also be driven by an analog buffer amplifier and the reception lines could be held at a constant voltage by a transimpedance amplifier. However, this would require additional components. By implementing the sensor readout via direct delta-sigma conversion, we can achieve good accuracy with minimal external components.

However, having to use relatively low excitation frequencies also reduces the current that is capacitively coupled from each row into each column. We take several measures to still achieve an acceptable signal-to-noise ratio. Excitation signals are transmitted on all rows simultaneously at different frequencies and all reception lines are sampled continuously, while all samples are digitally integrated. Depending on the application, we either place the readout board close to the sensor, or, if the readout board is located further away from the sensor, we amplify the excitation signals (e.g. to 18V, with additional circuitry for protection).

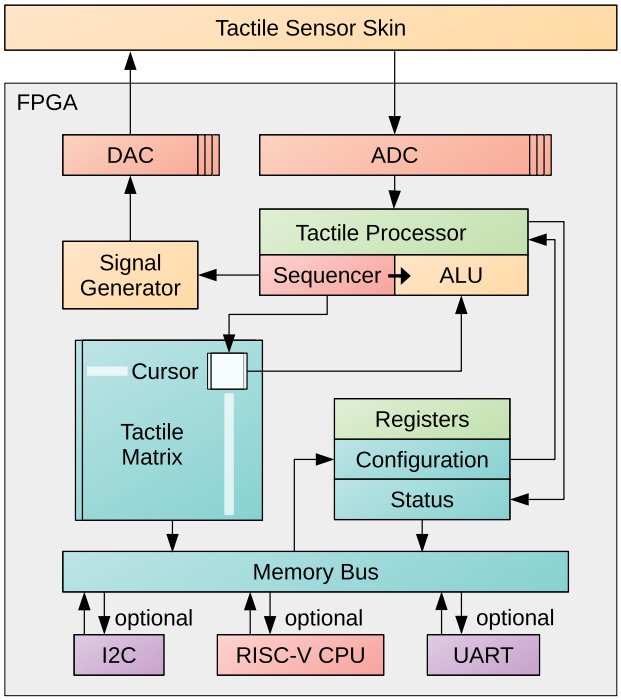

FIGURE 9. We develop a VLSI design for reading tactile sensor skin with minamal external components, integrating ADCs, DACs, signal generation, signal processing, and optionally a RISC-V CPU core and/or serial communication interfaces. The capacitance distribution across the tactile matrix is reconstructed in hardware, without any intervention from the CPU or host processor.

While on the one hand, the impedance characteristics of the conductive silicone require additional precautions to still ensure a good signal-to-noise ratio, on the other hand, it can also be exploited to simplify the readout electronics.

The delta-sigma ADCs and DACs run at 24 MHz and 1 MHz respectively. The rate-coded bitstream from the ADC is converted down to the sample rate (e.g. 10 Hz) using a rectangular window with a width equal to the sample period (e.g. 0.1 s, reciprocal of the sample rate).

VI. PCB DESIGNS

We develop two alternative circuit board designs, a miniaturized one for distributed systems and one with more channels for centralized architectures.

Our miniaturized version measures 12 mm × 16 mm and can, for example, be placed above the fingernail to read a fingertip sensor. Many of these boards could be distributed across a larger system and used together. The board carries a Lattice ICE5LP1K low-power FPGA in a QFN48 package, feedback resistors for the reception lines, decoupling capacitors, a 1.2V regulator for the FPGA core voltage, an LED for optical motion tracking, and a 6-axis IMU (ICM-42605). Eight contact pads at the bottom connect to the conductive silicone traces and support up to 16 sensor cells. The board can be connected to a host processor via four wires (power, ground, clock, data). During startup, the clock and data lines serve as a unidirectional SPI bus to transfer the configuration

bitstream to the FPGA. At runtime, the clock and data lines are used as a bidirectional I^2C bus.

Our second design (see figure 8) can simultaneously read 256 sensor cells via 16 output and 16 input channels. The board measures 30 mm × 33 mm. For a glove or robot hand, it could be placed on the back of the hand or on the wrist. The circuit is designed to read tactile sensors over a short distance via elastic cables made from electrically conductive silicone. To achieve a good signal-to-noise ratio despite limited conductivity, we increase the transmission voltage. A boost converter generates a higher supply voltage (currently 18V). One push-pull driver (MCP1415) for each output channel amplifies the corresponding binary delta-sigma-modulated bitstream. Due to the increased excitation voltage, we add additional protection circuitry. Input and output currents are limited by series resistors and input voltages are clamped via diode networks (DALC208SC6). We integrate a Lattice ECP5 LFE5U-12F FPGA to handle the increased workload and a configuration flash memory. The FPGA is large enough to fulfill additional functions, such as running an RISC-V softcore. A separate host microcontroller is not required. We also add eight GPIO pads, voltage regulators including an efficient step-down converter to power the FPGA core, a Micro JST connector with a JTAG port and an additional GPIO pin (e.g., serial port), a status LED with an embedded driver (WS2812B), and a crystal oscillator.

VII. VLSI DESIGN

We develop a configurable VLSI design for FPGAs or ASICS to read our tactile matrix sensors with minimal external components (see figure 9). Our design includes synthesizers for excitation signals, delta-sigma A/D and D/A converters, a processing unit to reconstruct a complex impedance matrix from row and column signals in hardware, a double-buffered memory for storing and safely accessing the tactile matrix, and a set of configuration and status registers. The memory and registers can be mapped into the address space of a host processor (e.g. a RISC-V core). For distributed architectures with a discrete host microcontroller, the same resources can also be accessed over an optional I2C bus without requiring a CPU on the readout chip.

For each excitation signal, we maintain a linear phase counter and generate sine and cosine functions. The sine waves are output via a delta-sigma D/A converter. At each input channel, a current-mode delta-sigma A/D converter keeps the voltage at a constant reference voltage to suppress crosstalk and, at the same time, measures the current that is coupled from the excitation lines into the reception lines. The tactile matrix processor is implemented as a state machine and continuously iterates over all taxels. It correlates the sines and cosines corresponding to the current cell with the input signal from the corresponding A/D converter and updates in-phase and quadrature counters in a complex-valued impedance matrix. At a regular swap interval, the tactile matrix is copied from an internal back buffer to a front buffer, which can be accessed by the host processor.

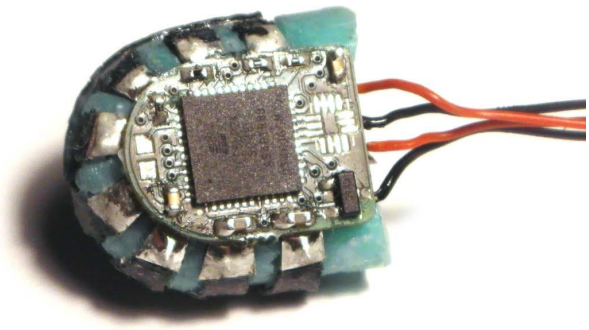

FIGURE 10. Multimodal fingertip sensor with elastic double-curved tactile skin and integrated readout electronics.

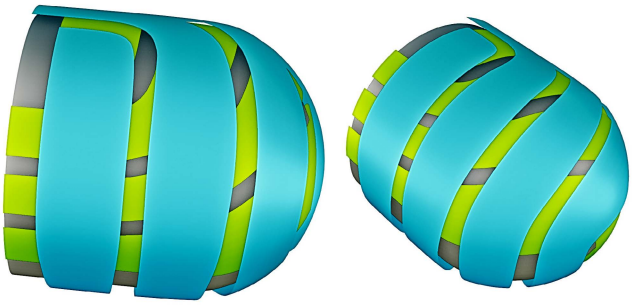

FIGURE 11. CAD model of the electrode layout for a double-curved fingertip sensor. Two sets of electrically conductive silicone traces wrap around the surface and form pressure-sensitive variable capacitors at the intersections.

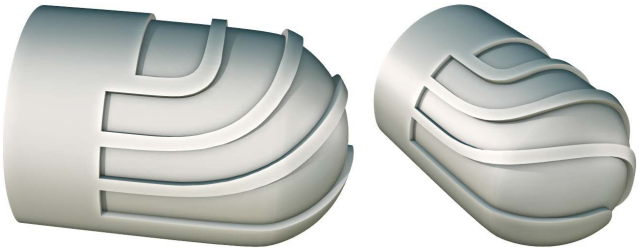

FIGURE 12. Computer-generated assembly jig for a tactile fingertip sensor. The parts are temporarily glued into the slots on the fixture and then applied to the skin, allowing for accurate placement.

Excitation and swap frequencies can be specified as ratios between clock multipliers and a clock divider. The data is available almost immediately after a sample period has ended, with a delay of less than 0.1 ms.

To synthesize the FPGA bitstream, we use Yosys [42], NextPNR [43], Project IceStorm [44] and Project Trellis [45].

VIII. PROTOTYPES

We present two prototypes to demonstrate different aspects of our technology. Both designs measure contact forces on a human finger and feature a double-curved tactile matrix that wraps around a finger tip. The skins can stretch without damage to adapt to the diameter of the finger and to deformations under pressure. One design integrates the readout board locally on the finger tip. The other prototype covers the entire finger, can also sense contacts on the middle and proximal phalanges, and reads the tactile cells via an elastic silicone

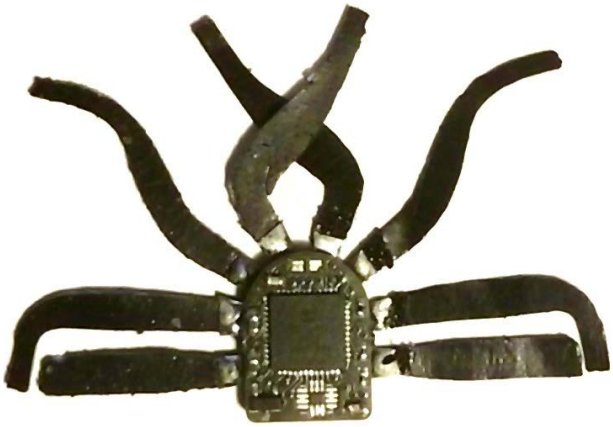

FIGURE 13. Elastic silicone traces soldered to a readout board.

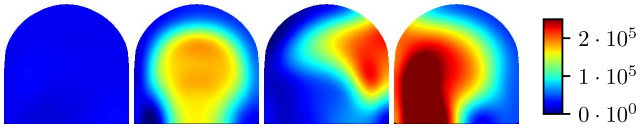

FIGURE 14. Force distributions measured by the tactile sensor matrix while wearing our multimodal fingertip on a human finger, without (left) and with contacts (middle, right).

cable. Each sensor can be used as a wearable device on a human finger or be glued to a humanoid robot hand.

A. MULTIMODAL FINGERTIP

We build a multimodal wearable sensor with a curved and elastic tactile skin that wraps around the fingertip. See figure 10 for a photo of the assembled sensor and figure 11 for a CAD model of the electrode layout. The matrix has 16 individual force-sensing taxels. We cast a conductive silicone sheet (table 2, column A), mold a closed-celled dielectric structure (figure 6), cut the sheet into pads with a cutting plotter and glue the pads to a 3D-printed assembly jig (figures 6 and 12). A small circuit board (section VI) is placed above the finger nail, with readout electronics as well as an LED and a 6-axis IMU for motion tracking. The elastic silicone traces are connected to the circuit board by attaching small metal pads (section III-I, table 2B) and soldering the pads to the circuit board. See figure 13 for an image of the elastic conductors soldered to the readout board. Even if only held by the soldered metal pad, the conductive silicone can be stretched without damaging the part or joint, as shown in figure 7. We connect the readout board using four wires for power, ground, data and clock to an ESP32 microcontroller. See figure 14 for a visualization (as described in appendix XI) of exemplary tactile readings when worn on a human fingertip and figure 15 for a multimodal time series with tactile, accelerometer and gyroscope data.

B. FINGER SENSOR

We build a second prototype that covers an entire finger and can also detect contacts on the middle and proximal phalanges. The sensor is connected to the readout board through an elastic silicone cable (section III-G, table 2D),

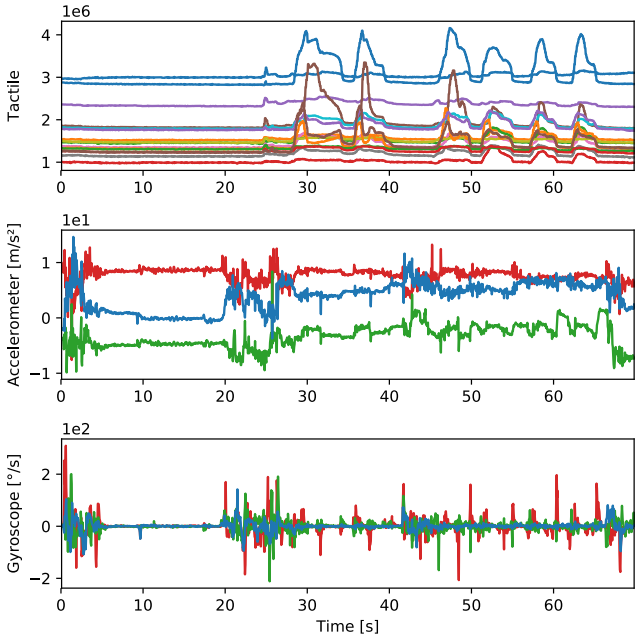

FIGURE 15. Tactile data (top) with corresponding accelerometer (middle) and gyroscope (bottom) readings while wearing a multimodal fingertip sensor with an elastic sensor skin on a human hand and manipulating objects. Each line in the tactile plot represents one taxel, corresponding to a specific location on the fingertip.

which runs along the top of the finger and extends far enough for the readout board to be placed on the wrist. See figure 2 for sensor layout, assembly jig and dielectric mold. All parts on the finger and hand are made from elastic silicone (section IV-B, IV-C, IV-D, table 2C, 2D, 2E). It is highly stretchable and the same sensor can fit onto different fingers, as shown in figure 18. The dielectric has an open cell structure. Cable and sensor are joined through vertical vias (section III-H).

We want to keep the skin on the insides of the joints as thin as possible for maximum flexibility. We therefore contact the sensor cells on the middle and proximal links only from the sides. Each of these sensor rings effectively forms a 2-by-2 matrix with 3 active taxels. To not waste any space in the logical sensor matrix and to avoid redundant traces, we combine the two sensor rings on the middle and proximal links into a logical 2-by-3 matrix.

Figure 16 shows tactile readings during object manipulation when the sensor is worn on a human finger. Our sensor skin produces consistent results even when the finger is bent. We can also use it on a robot finger, as shown in figure 17. The visualizations are generated as described in appendix XI. The same sensor works on human and robot fingers with different shapes and sizes. Instead of having to integrate and connect individual sensors on each robot link, we can use a single sensor skin that stretches around the entire finger and even around joints.

IX. CALIBRATION

We place a piece of sensor skin on top of a load cell, apply different amounts of pressure and capture the outputs of the

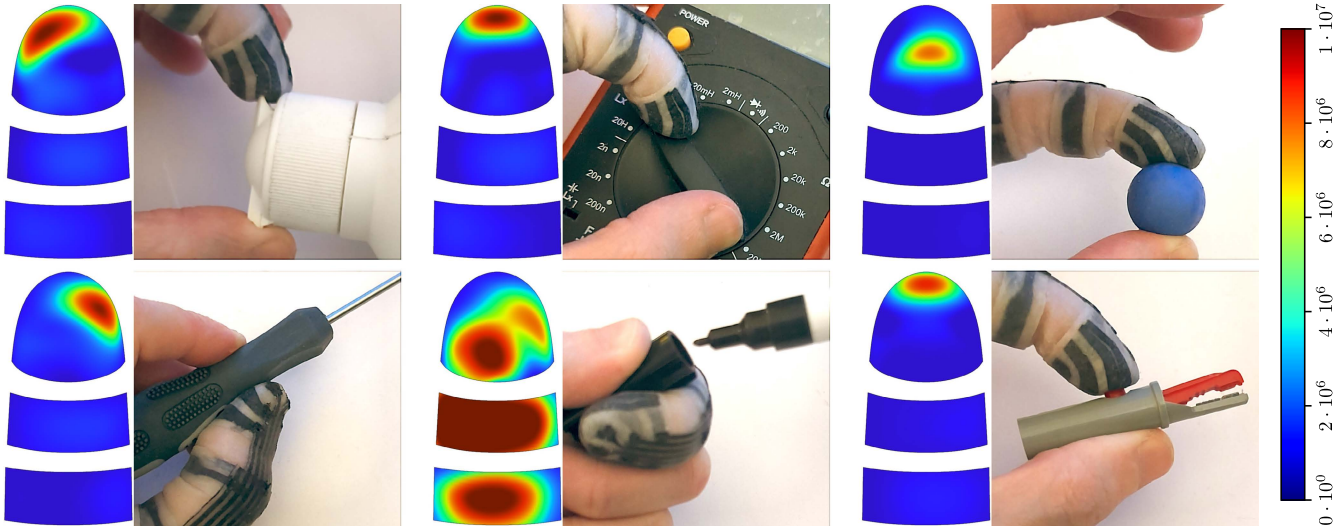

FIGURE 16. Our tactile finger sensor measures contacts on the distal, middle and proximal phalanges during manipulation tasks. It can stretch to fit on different fingers and still produce meaningful data. Opening a bottle (top-left, sensor on first finger), operating an LC meter (top-center, first finger), holding a rubber ball (top-right, little finger), holding a screwdriver (bottom-left, thumb), opening a permanent marker (bottom-center, first finger), using a testclip (bottom-right, first finger).

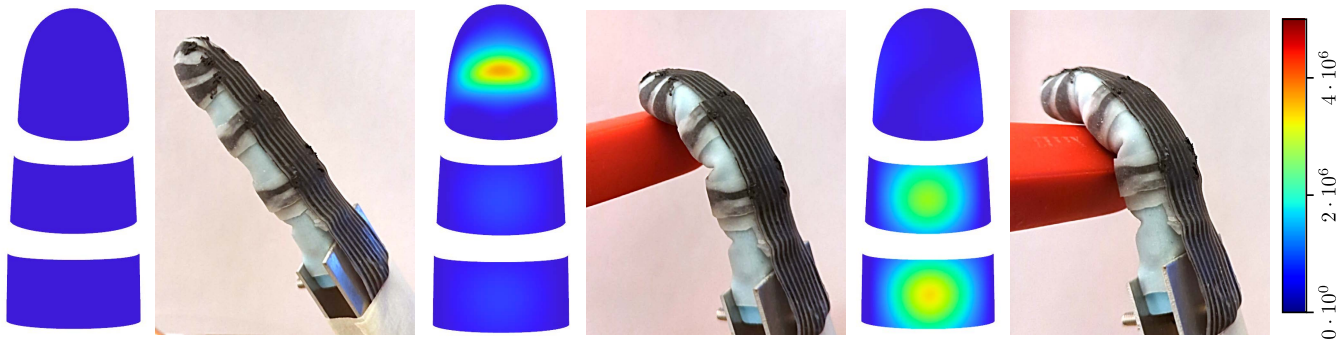

FIGURE 17. Tactile sensor skin is placed on a humanoid robot finger and measures contact information.

tactile readout board and of a load cell amplifier (HX-711). The pressure is applied to a cell with a size of 1 cm × 1 cm. We find that the characteristics can be approximated well by a simple rational function with three parameters a, b, c.

$$y = \frac{a}{b + c \cdot x} \tag{1}$$

We fit the model by minimizing a least-squares loss. See figure 19 for a plot of the data and of the model.

X. CHARACTERIZATION

We measure the response of a piece of tactile skin to different stimuli. The sensor has a cell size of 5 mm × 5 mm. It is connected to a readout board via a 7 cm long elastic silicone cable with a pitch of 1 mm and a trace width of 0.5 mm. Unless stated otherwise, we set the integration time to 0.1 s, corresponding to a sample rate of 10 Hz.

We place a small weight with a mass of 1 g and a radius of 5 mm on randomly selected sensor cells. See figure 20 for an exemplary timeplot. The noise corresponds to a standard deviation of approximately 0.19 g. We repeat the experiment several times for multiple different sensor cells and compute averages, medians, quartiles, and 5 % quantiles (figure 23b). The 1 g weight can be detected reliably, even across different cells (figure 23a,b). Heavier weights lead to stronger responses (figure 23c,d,e). To make the results easier to compare, we apply the pressures to areas of equal size using a small circular stamp with a diameter of 5 mm.

We record a second timeplot using a larger weight with a mass of 50 g and a diameter of 2 cm, placing the weight directly onto the sensor skin and then removing it. See figure 21 for results. The measurements show no significant hysteresis and settle within two samples.

We further test the behavior under changing contacts by rolling a 2€ coin across the sensor and plotting the response (figure 22). Each output along the affected path reaches a similar maximum, showing good consistency across different cells (as in figure 23). When the object is located between the centers of two cells, the measurements show a smooth transition, which might be usable for sub-pixel localization.

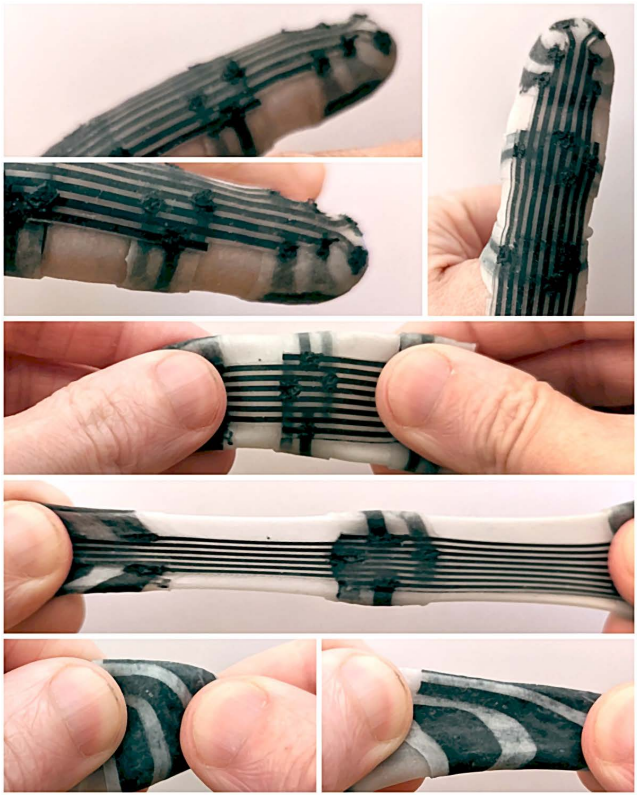

FIGURE 18. The same elastic finger sensor fits the little finger, first finger and thumb. It can be stretched without damage.

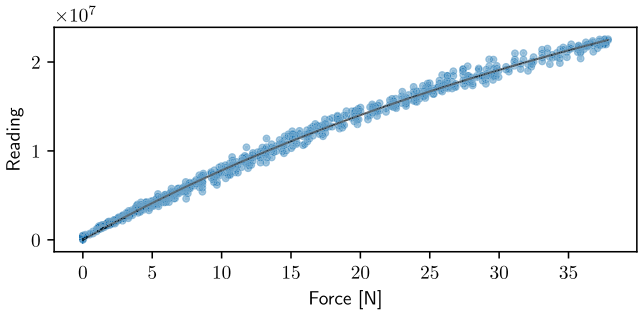

FIGURE 19. We apply different contact forces to a piece of tactile sensor skin and measure the response (blue dots). The behavior can be approximated by a simple model (black line).

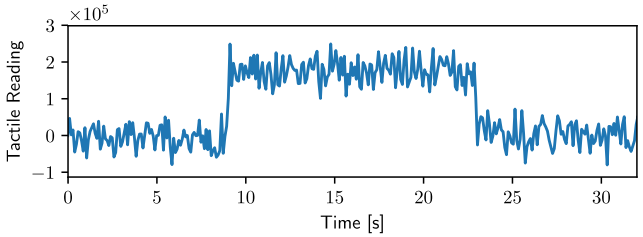

FIGURE 20. Tactile readings while placing a 1 g weight on a piece of sensor skin and removing it, with an integration time of 0.1 s and a cell size of 5 mm.

Capacitive sensors can suffer from electrical interference in the proximity of materials with a high dielectric permittivity, such has human fingers. Placing our sensor matrix on a human finger (figure 23f) does not lead to a significant bias. It only results in slightly increased noise, but the accuracy is still better than 1 g (figure 23b,f).

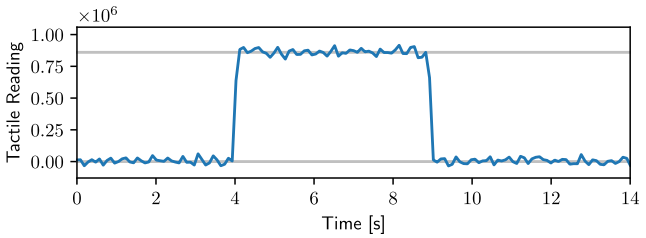

FIGURE 21. We place a circular weight with a diameter of 2 cm and a mass of 50 g on a piece of tactile skin with a cell size of 0.5 cm and plot readings from one of the cells over time.

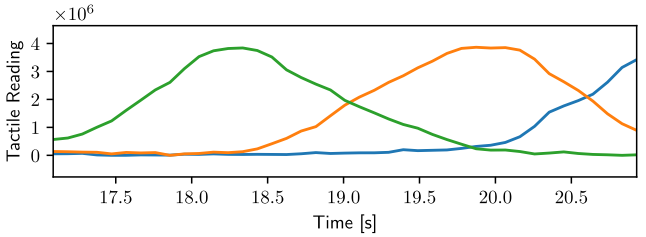

FIGURE 22. Tactile readings from three different sensor cells during a rolling contact.

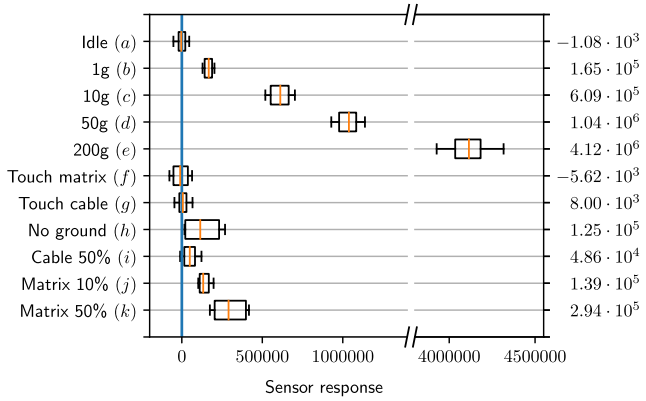

FIGURE 23. We measure the response (X axis) of a piece of tactile sensor skin with a cell size of 0.5 cm and a 7 cm long silicone cable to different stimuli (Y axis). Each measurement is performed multiple times for different cells to determine averages (right), medians (orange), first and third quartiles (boxes), and 5 % quantiles (whiskers).

Touching the cable with a human finger does usually not significantly affect the measurements (figure 23g). However, if a transmission line and a reception line are placed directly next to each other and a human finger touches the same spot, a slight response (equivalent to 1 g or less) can be measured (figure 23h). This only significantly affects one cell that is connected to these two traces. The effect can be easily suppressed by routing transmission and reception lines as separate groups and placing a single ground trace or an unused reception line (current-mode ADC) in between (equivalent to figure 23g).

Both the cable and the sensor are made from elastic silicone. Stretching the cable leads to a small response, but the effect is minimal. If we stretch a 6 cm long part of the cable by 50 % to a length of 9 cm, the error is still significantly below an equivalent of 1 g (figure 23b,i). Stretching one of the sensor cells by 10 % can lead to an offset of slightly below 1 g

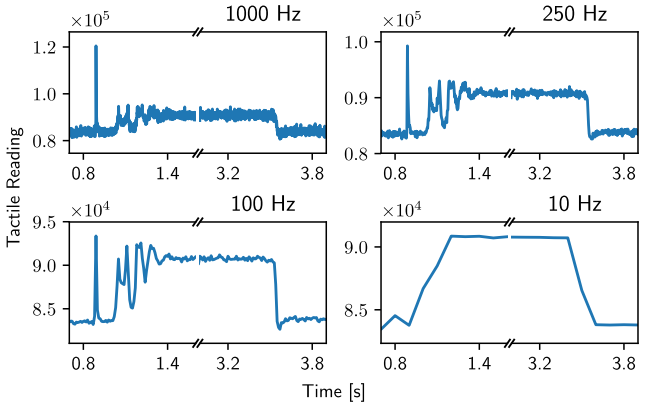

FIGURE 24. The dynamic response can be configured depending on the application. We drop a 20 g weight onto a piece of sensor skin and process the same bitstream with different integration times and sample rates. Higher sample rates can detect fast transients (top) while longer integration times lead to more stable measurements (bottom).

(figure 23b,j), stretching a cell by 50 % can lead to an offset of up to a few grams (figure 23b,c,k).

For our current uses on human and robot hands, these effects are either negligible or can be easily mitigated (figures 16, 17). The sensor cells may by stretched when a different human wearer first puts a sensor glove on. This can be compensated by re-initializing the zero offset before use. We measure the change in diameter of different human fingers under bending. All values are below 10 %. In this range, deviations from stretching the sensor cells should be negligible for our applications, which is also confirmed qualitatively by our manipulation experiments (section VIII). We expect the largest amount of stretching in the cable that runs along the top of the finger and around joints. Stretching the cable has a negligible effect on the measurements.

Some of the trials with the 1 g weight were performed before the other experiments, some immediately afterwards, and some were performed 5 days later (figure 23b), showing good stability even under higher loadings and stretching.

The dynamic response can be configured depending on the application. We drop a small weight of 20 g from a height of 1 cm onto a piece of sensor skin with a cell size of 5 mm × 5 mm and lift it off. The weight is dropped at an angle and first bounces back and forth before it settles. We process the same 24 MHz ADC bitstream for a single sensor cell with different integration times and sample rates, ranging from 1 ms or 1 kHz to 100 ms or 10 Hz. With a small integration time and high sample rate, we can capture fast transients when the object first makes contact (see figure 24, top). The first peak is significantly dampened at integration times of 4 ms and higher, suggesting a mechanical bandwidth of at least 100 Hz. Larger integration times can dampen both noise and mechanical transients, and can lead to more stable measurements (see figure 24, bottom).

XI. CONCLUSION AND FUTURE WORK

We can produce tactile sensor skin that wraps around double-curved surfaces and stretches with underlying soft parts and joints. While previous technologies are missing essential features needed for our future work in robotic manipulation, our new sensor skin fulfills our requirements. It is robust and elastic enough to wrap tightly around a human finger while still producing meaningful data. It can detect multiple simultaneous contacts and shows good accuracy, repeatability and dynamic response. The same sensor can be worn on different fingers with different diameters and fingertip radii, suggesting that the same wearables could be used to record human demonstrations for imitation learning from many different human teachers, without having to individually customize the hardware. Unlike traditional flat matrices, our double-curved sensors can measure contacts also on the front and sides, even for rolling contacts. The devices are thin and elastic enough for a human wearer to feel the objects they are manipulating, which is considered essential to study how humans use their own sense of touch.

In our future work, we want to build multimodal sensor gloves from only elastic materials, record new datasets for imitation learning, integrate our tactile skin on robots, and continue our work on robotic dexterous manipulation. We are particularly interested in multimodal fusion to detect and control physical contacts.

APPENDIX A
ACRONYMS

ADC . . . . Analog-to-digital converter
ALU . . . . Arithmetic logic unit
ASIC . . . . Application-specific integrated circuit
CAD . . . . Computer-aided design
CAS . . . . . Chemical Abstracts Service
CPU . . . . . Central processing unit
CNC . . . . Computer numerical control
DAC . . . . Digital-to-analog converter
DMS . . . . Dimethylsiloxane
FFF . . . . . Fused filament fabrication
FPGA . . . Field programmable gate array
I2C . . . . . Inter-integrated circuit
IMU . . . . . Inertial measurement unit
LED . . . . . Light-emitting diode
LVDS . . . Low-voltage differential signaling
PCM . . . . Pulse-code modulation
PDMS . . . Polydimethylsiloxane
PLA . . . . . Polylactic acid
PTFE . . . Polytetrafluoroethylene
QFP . . . . . Quad flat package
RC . . . . . Resistor–capacitor
RISC . . . . Reduced instruction set computer
UART . . . Universal asynchronous receiver-transmitter

APPENDIX B
PACKING

After unwrapping, we want to pack all parts into a small area to minimize waste. While bin packing is a common problem, popular open-source libraries are restricted to special cases, such as rectangles [46], [47] or convex shapes [48].

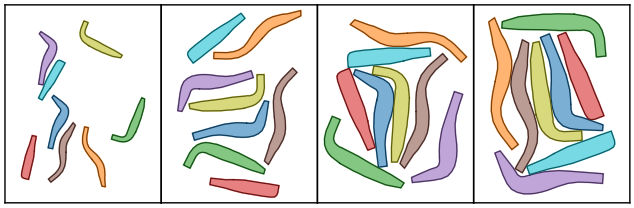

FIGURE 25. The conductive parts for a fingertip sensor are arranged to minimize waste during manufacture (left to right).

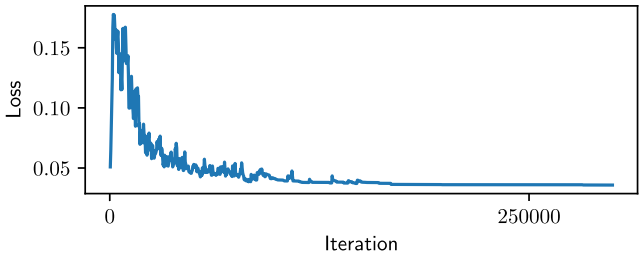

FIGURE 26. Our packing algorithm arranges conductive parts for efficient manufacture by minimizing the required area (Y axis) over multiple iterations (X axis) while avoiding overlap.

For our application, the parts are often highly non-convex. We develop a custom non-convex bin packer. The problem is formulated as a constrained optimization problem with free variables P, A for part positions and orientations. We minimize the area $w \cdot h$ of the bounding rectangle while ensuring that the pairwise overlap $o_{i,j}$ between all parts i, j is zero.

$$\underset{P,A}{\text{minimize}}\ w \cdot h \qquad s.t. \sum_{i,j} o_{i,j} = 0 \tag{2}$$

We implement a combined loss as an ordered pair and solve the problem through simulated annealing (see figures 25 and 26).

APPENDIX C
VISUALIZATION

Our sensor skin is read as a two-dimensional matrix. If it consists of different physically disconnected parts, we first split the data into different segments. To convert the data into an image, we apply a bicubic interpolation and a color map using OpenCV [49]. If the sensor has an irregular or curved shape, we generate a polygon mesh along the conductive traces and assign texture coordinates according the the row and column indices. The mesh is interpolated as a subdivision surface and projected onto the surface model (see section III-B). We then use the interpolated texture coordinates to map the previously generated image onto the surface model of the sensor skin. The colored surface model is published as a ROS [50], [51] message and rendered using TAMSVIZ [52]. The color bars and other plots are generated using Matplotlib [53].

REFERENCES

[1] S. R. Dahiya, G. Metta, M. Valle, and G. Sandini, "Tactile sensing—From humans to humanoids," *IEEE Trans. Robot.*, vol. 26, no. 1, pp. 1–20, Feb. 2010.

[2] H. Yousef, M. Boukallel, and K. Althoefer, "Tactile sensing for dexterous in-hand manipulation in robotics—A review," *Sens. Actuators A, Phys.*, vol. 167, no. 2, pp. 171–187, 2011.

[3] Z. Kappassov, J.-A. Corrales, and V. Perdereau, "Tactile sensing in dexterous robot hands—Review," *Robot. Auton. Syst.*, vol. 74, pp. 195–220, Dec. 2015.

[4] A. J. Fishel, J. V. Santos, and E. G. Loeb, "A robust micro-vibration sensor for biomimetic fingertips," in *Proc. 2nd IEEE RAS EMBS Int. Conf. Biomed. Robot. Biomechtron.*, Oct. 2008, pp. 659–663.

[5] *Tekscan*. Accessed: Apr. 4, 2022. [Online]. Available: https://www.tekscan.com/

[6] B. Nie, R. Li, J. Brandt, and T. Pan, "Iontronic microdroplet array for flexible ultrasensitive tactile sensing," *Lab Chip*, vol. 14, pp. 1107–1116, Jan. 2014.

[7] S. Sundaram, P. Kellnhofer, Y. Li, J.-Y. Zhu, A. Torralba, and W. Matusik, "Learning the signatures of the human grasp using a scalable tactile glove," *Nature*, vol. 569, no. 7758, pp. 698–702, 2019.

[8] G. Büscher, R. Kõiva, C. Schürmann, R. Haschke, and H. J. Ritter, "Tactile dataglove with fabric-based sensors," in *Proc. 12th IEEE-RAS Int. Conf. Humanoid Robots (Humanoids)*, Nov. 2012, pp. 204–209.

[9] M. Zenker, R. Kõiva, and R. Haschke, *Shadow Hand Tactile Fingertip*. Accessed: Apr. 4, 2022. [Online]. Available: https://ni.www.techfak.uni-bielefeld.de/tactile/fingertip

[10] E. Battaglia, M. Bianchi, A. Altobelli, G. Grioli, G. M. Catalano, A. Serio, M. Santello, and A. Bicchi, "Thimblesense: A fingertip-wearable tactile sensor for grasp analysis," *IEEE Trans. Haptics*, vol. 9, no. 1, pp. 121–133, Jan. 2016.

[11] W. Yuan, S. Dong, and E. H. Adelson, "Gelsight: High-resolution robot tactile sensors for estimating geometry and force," *Sensors*, vol. 17, no. 12, p. 2762, 2017.

[12] P. Mittendorfer and G. Cheng, "Uniform cellular design of artificial robotic skin," in *Proc. 7th German Conf. Robot.*, 2012, pp. 1–5.

[13] H.-K. Lee, S.-I. Chang, and E. Yoon, "A flexible polymer tactile sensor: Fabrication and modular expandability for large area deployment," *Microelectromech. Syst., J.*, vol. 15, no. 6, pp. 1681–1686, Dec. 2006.

[14] M. Lambeta, G. Kammerer, D. Jayaraman, R. Calandra, P.-W. Chou, S. Tian, B. Yang, B. Maloon, V. Most, D. Stroud, R. Santos, and A. Byagowi, "Digit: A novel design for a low-cost compact high-resolution tactile sensor with application to in-hand manipulation," *IEEE Robot. Automat. Lett.*, vol. 5, no. 3, pp. 3838–3845, Feb. 2020.

[15] H. Sun, J. K. Kuchenbecker, and G. Martius, "A soft thumb-sized vision-based sensor with accurate all-round force perception," *Nature Mach. Intell.*, vol. 4, pp. 135–145, Feb. 2022.

[16] P. Ruppel and J. Zhang, "Learning object manipulation with dexterous hand-arm systems from human demonstration," in *Proc. IEEE/RSJ Int. Conf. Intell. Robots Syst. (IROS)*, Jan. 2021, pp. 5417–5424.

[17] N. Fiedler, P. Ruppel, Y. Jonetzko, N. Hendrich, and J. Zhang, "A low-cost modular system of customizable, versatile, and flexible tactile sensor arrays," in *Proc. IEEE/RSJ Int. Conf. Intell. Robots Syst. (IROS)*, Oct. 2021, pp. 1771–1777.

[18] P. Ruppel, Y. Jonetzko, M. Görner, N. Hendrich, and J. Zhang, "Simulation of the SynTouch BioTac sensor," in *Proc. 15th Int. Conf. (IAS)*. Cham, Switzerland: Springer, Jan. 2019, pp. 374–387.

[19] S. Y. Narang, B. Sundaralingam, K. V. Wyk, A. Mousavian, and D. Fox, "Interpreting and predicting tactile signals for the SynTouch BioTac," 2021, *arXiv:2101.05452*.

[20] F. Wang, H. Liu, F. Sun, and H. Pan, "Fabric recognition using zero-shot learning," *Tsinghua Sci. Technol.*, vol. 24, pp. 645–653, Dec. 2019.

[21] Y. Wang, W. Huang, B. Fang, and F. Sun, "Elastic interaction of particles for robotic tactile simulation," 2020, *arXiv:2011.11528*.

[22] N. F. Lepora, "Soft biomimetic optical tactile sensing with the TacTip: A review," *IEEE Sensors J.*, vol. 21, no. 19, pp. 21131–21143, Oct. 2021.

[23] J. E. Nicolson and S. R. Fearing, "Sensing capabilities of linear elastic cylindrical fingers," in *Proc. IEEE/RSJ Int. Conf. Intell. Robots Syst. (IROS)*, vol. 1, Aug. 1993, pp. 178–185.

[24] PPS Medical Tactile Inc. *TactileGlove—Hand Pressure and Force Measurement*. Accessed: Apr. 5, 2022. [Online]. Available: https://pressureprofile.com/body-pressure-mapping/tactileglove

[25] J. Shintake, E. Piskarev, S. H. Jeong, and D. Floreano, "Ultrastretchable strain sensors using carbon black-filled elastomer composites and comparison of capacitive versus resistive sensors," *Adv. Mater. Technol.*, vol. 3, no. 3, 2018, Art. no. 1700284.

[26] G. Gu, H. Xu, S. Peng, L. Li, S. Chen, T. Lu, and X. Guo, "Integrated soft ionotronic skin with stretchable and transparent hydrogel-elastomer ionic sensors for hand-motion monitoring," *Soft Robot.*, vol. 6, no. 3, pp. 368–376, Jun. 2019.
[27] R. Zuo, Z. Zhou, B. Ying, and X. Liu, "A soft robotic gripper with anti-freezing ionic hydrogel-based sensors for learning-based object recognition," in *Proc. IEEE Int. Conf. Robot. Automat. (ICRA)*, May 2021, pp. 1–6.
[28] C. Thrasher, Z. Farrell, N. Morris, C. L. Willey, and C. Tabor, "Mechanoresponsive polymerized liquid metal networks," *Adv. Mater.*, vol. 31, Aug. 2019, Art. no. 1903864.
[29] P. Mason, F. Uhlig, V. Vaněk, T. Buttersack, S. Bauerecker, and P. Jungwirth, "Coulomb explosion during the early stages of the reaction of alkali metals with water," *Nature Chem.*, vol. 7, pp. 4–250, Mar. 2015.
[30] R. Arvidsson, M. Boholm, M. Johansson, and M. Montoya, "Just carbon': Ideas about graphene risks by graphene researchers and innovation advisors," *NanoEthics*, vol. 12, pp. 199–210, Dec. 2018.
[31] K. Sanderson, "Carbon nanotubes: The new asbestos?" *Nature*, 2008, doi: 10.1038/news.2008.845.
[32] W. Wang, S. Wang, R. Rastak, Y. Ochiai, S. Niu, Y. Jiang, P. Arunachala, J. Xu, N. Matsuhisa, X. Yan, S.-K. Kwon, M. Miyakawa, Z. Zhang, R. Ning, A. Foudeh, Y. Yun, C. Linder, J. Tok, and Z. Bao, "Strain-insensitive intrinsically stretchable transistors and circuits," *Nature Electron.*, vol. 4, pp. 1–8, Feb. 2021.
[33] N. S. Danial, M. M. Ramli, D. S. C. Halin, H. Hong, S. M. S. Isa, M. M. A. B. Abdullah, N. M. Asyikin Anhar, L. F. A. Talip, and N. S. Mazlan, "Incorporation of polydimethylsiloxane with reduced graphene oxide and zinc oxide for tensile and electrical properties," in *Proc. AIP Conf.*, vol. 1887, no. 1. New York, NY, USA: AIP, Sep. 2017.
[34] C. M. Boutry, Y. Kaizawa, B. C. Schroeder, A. Chortos, A. Legrand, Z. Wang, J. Chang, P. Fox, and Z. Bao, "A stretchable and biodegradable strain and pressure sensor for orthopaedic application," *Nature Electron.*, vol. 1, no. 5, pp. 314–321, May 2018.
[35] P. Mazurek, S. Vudayagiri, and A. L. Skov, "How to tailor flexible silicone elastomers with mechanical integrity: A tutorial review," *Chem. Soc. Rev.*, vol. 48, no. 6, pp. 1448–1464, 2019.
[36] B. Arkles, J. Goff, S. Sulaiman, and A. Phillips, "Ultra-high elongation silicone elastomers," *Rubber World*, vol. 254, pp. 29–34, Jun. 2016.
[37] J. Goff, S. Sulaiman, B. Arkles, and P. J. Lewicki, "Soft materials with recoverable shape factors from extreme distortion states," *Adv. Mater.*, vol. 28, no. 12, pp. 2393–2398, Jan. 2016.
[38] P. Ruppel, N. Hendrich, and J. Zhang, "Direct policy optimization with differentiable physical consistency for dexterous manipulation," in *Proc. IEEE Int. Conf. Robot. Biomimetics (ROBIO)*, Dec. 2021, pp. 650–655.
[39] NinjaTek Fenner Inc. *Ninjaflex Eel, Fully Conductive, Flexible Filament for 3D Printers*. Accessed: Mar. 29, 2022. [Online]. Available: https://ninjatek.com/shop/eel/
[40] Troll Factory. *Silikon Kautschuk Typ 2 Abformsilikon mittelhart, TFC4010*. Accessed: Mar. 29, 2022. [Online]. Available: https://trollfactory.de/
[41] R. Moučka, M. Sedlačík, J. Osička, and V. Pata, "Mechanical properties of bulk Sylgard 184 and its extension with silicone oil," *Sci. Rep.*, vol. 11, no. 1, Sep. 2021, Art. no. 19090.
[42] C. Wolf. *Yosys Open SYnthesis Suite*. Accessed: Mar. 29, 2022. [Online]. Available: https://yosyshq.net/yosys/
[43] D. Shah, E. Hung, C. Wolf, S. Bazanski, D. Gisselquist, and M. Milanovic, "Yosys+nextpnr: An open source framework from verilog to bitstream for commercial FPGAs," in *Proc. IEEE 27th Annu. Int. Symp. Field-Program. Custom Comput. Mach. (FCCM)*, Apr. 2019, pp. 1–4. Accessed: Mar. 29, 2022.
[44] C. Wolf and M. Lasser. *Project IceStorm, Open Source Verilog-Tobitstream Flow for Ice40 FPGAs*. Accessed: Mar. 29, 2022. [Online]. Available: http://bygone.clairexen.net/icestorm/
[45] *Project Trellis*. Accessed: Mar. 29, 2022. [Online]. Available: https://github.com/YosysHQ/prjtrellis
[46] M. Iori, V. L. D. Lima, S. Martello, and M. Monaci, "2DPackLib: A two-dimensional cutting and packing library," *Optim. Lett.*, vol. 16, pp. 1–10, Mar. 2022.
[47] T. Skjølberg. *3D-Bin-Container-Packing*. Accessed: Mar. 29, 2022. [Online]. Available: https://github.com/skjolber/3d-bin-container-packing
[48] T. Meszaros. *Libnest2D, a Library and Framework for the 2D Bin Packaging Problem*. Accessed: Mar. 29, 2022. [Online]. Available: https://github.com/tamasmeszaros/libnest2d
[49] G. Bradski, "The OpenCV library," *Dr. Dobb's J. Softw. Tools*, vol. 25, no. 11, pp. 120–123, 2000.
[50] M. Quigley, B. Gerkey, K. Conley, J. Faust, T. Foote, J. Leibs, E. Berger, R. Wheeler, and A. Ng, "ROS: An open-source robot operating system," in *Proc. ICRA Workshop Open Source Softw.*, 2009, pp. 1–6.
[51] *Robot Operating System*. Accessed: Jun. 24, 2022. [Online]. Available: https://www.ros.org/
[52] P. Ruppel. *TAMSVIZ—Visualization and Annotation Tool for ROS*. Accessed: Jun. 24, 2022. [Online]. Available: https://github.com/TAMS-Group/tamsviz
[53] J. D. Hunter, "Matplotlib: A 2D graphics environment," *Comput. Sci. Eng.*, vol. 9, no. 3, pp. 90–95, May/Jun. 2007.

PHILIPP RUPPEL received the B.Sc. and M.Sc. degrees in informatics from Universität Hamburg, Germany, in 2014 and 2017, respectively. He is currently a Research Associate with the Department of Informatics, Universität Hamburg. His research interests include robotics, machine learning, and dexterous manipulation.

NORMAN HENDRICH received the B.Sc. and M.Sc. degrees in physics and the Ph.D. degree in computer science from the University of Hamburg, Germany, in 1986, 1991, and 1996, respectively. He is currently a Senior Lecturer with the Department of Informatics, University of Hamburg. He has participated as a Principal Investigator in several collaborative European research projects and also acts as the Project Manager of the joint Sino-German Project Transregio-SFB TRR169 Crossmodal Learning. His research interests include computer simulation and machine learning, with a focus on applications in service robotics and dexterous manipulation.

JIANWEI ZHANG received the Bachelor of Engineering (Hons.) and Master of Engineering degrees from the Department of Computer Science, Tsinghua University, Beijing, China, in 1986 and 1989, respectively, the Ph.D. degree from the Department of Computer Science, Institute of Real-Time Computer Systems and Robotics, University of Karlsruhe, Germany, in 1994, and the Habilitation degree from the Faculty of Technology, University of Bielefeld, Germany, in 2000. He is currently a Professor and the Director of the Group TAMS, Department of Informatics, University of Hamburg, Germany. His research interests include sensor fusion, intelligent robotics, and multimodal machine learning. In these areas, he has published about 400 journal and conference papers, technical reports, and four books. He received multiple best paper awards. He is the Coordinator of the DFG/NSFC Transregional Collaborative Research Centre SFB/TRR169 Crossmodal Learning and several EU robotics projects. He is a life-long Academician of the Academy of Sciences in Hamburg. He was a member of the IEEE Robotics and Automation Society AdCom, from 2013 to 2015. He is the General Chair of IEEE MFI 2012, IEEE/RSJ IROS 2015, and the International Symposium of Human-Centered Robotics and Systems 2018.